Forecasting for Future CMB Searches for Primordial Magnetic Fields
Literature Review

University of Melbourne

Dylan Sutton
Supervised by Dr. Christian Reichardt

27th May 2016

Abstract

Contents

1 Introduction

ΛCDM cosmology is very successful at describing the Universe. However there remain many outstanding problems in the model that beg for a solution. One problem is the mysterious origin of the large-scale magnetic fields permeating the cosmos. Detections of Faraday rotation, synchrotron emissions and Zeeman splitting in distant galaxies and throughout intracluster media reveal weak magnetic fields, on the order of microgauss coherent over the scale of megaparsecs. Though there are models for describing the amplification of existing magnetic fields, such as magnetohydrodynamics and galactic dynamos there is no clear answer for where these magnetic fields came from.

A possible answer to this question are primordial magnetic fields (PMFs). PMFs are seed magnetic fields produced in the early Universe sometime before recombination. These weak seed fields - of order nanoguass - could be taken up by galactic dynamos to become the weak magnetic field we see today. So far PMFs remain undetected, but with the next generation of CMB experiments and beyond beginning over the next decade, it is important to know how sensitive these experiments are to the faint traces of PMFs and whether they are able to make a detection. The aim of this thesis is to forecast the upper-limits on PMF detections for stage-3 and stage-4-like CMB experiments.

In this chapter I will begin by discussing the nature of the large-scale magnetic fields and the physics behind their amplification due to galactic dynamos in section 2.1. In section 2.2 I will discuss recent advances in constraining the PMF strength. Next, in section 2.3 I will give a quick review on CMB observables, polarisation and power spectra - which are instrumental in the study of PMFs. Finally in section 2.4 I will discuss CMB-S3 experiments with focus on the SPT-3G and Advanced ACTPol as well as preliminary figures on CMB-S4 experiments.

1.1 Large Scale Magnetic Fields

Galaxy clusters and their resident galaxies are known to possess weak microgauss magnetic fields coherent over scales as large as megaparsecs. Observational evidence of these magnetic fields come in the form of Zeeman splitting, synchrotron emission and Faraday rotation.

Zeeman Splitting

In the presence of magnetic fields, electronic energy levels in molecules and atoms split based on the angular momentum of the electron with respect to the orientation of the magnetic field. As a result, Zeeman splitting causes the spectral lines from distant sources to also split. Splitting of the Hydrogen 21cm line and the OH 18cm line are common probes of magnetic fields in our owng galaxy. Currently Zeeman splitting has given no constraints on the magnetic fields in the ICM. Zeeman splitting has been used to measure the magnetic fields within dense gas clouds around other galaxies, with strengths in the order of 0.5-18mG [1], however these regions are not representative of the large-scale magnetic fields threading the cosmos.

Synchrotron Emissions

As electrons and ions spiral around magnetic fields in galaxies and the intracluster medium they emit synchrotron radiation with energies proportional to the strength of the magnetic field and the velocity of the ions.
The emissivity of synchrotron radiation is given by:

$$j(B_\perp, \nu) \propto n_0 B_\perp^{(1+\alpha)/2} \nu^{(1-\alpha)/2} \tag{1}$$

Where ν is the frequency of the electron's circular motion, $B_\perp$ is the magnetic field component perpendicular to the line of sight and n_0 is the normalised electron density, given by $n_e dE = n_0 E^{-\alpha} dE$ where E is the energy of the electron and α is the spectral index, the value for which varies from galaxy to galaxy.
Synchrotron emissions from nearby galaxies have given constraints on $B_\perp$ within the range 4 μG to 19 μG [2].

Faraday Rotation

As a polarised photon travels through a magnetised plasma it undergoes Faraday Rotation. Magnetised plasmas such as the intracluster medium exhibit different refractive indices for left and right circularly polarised light. Hence, as linearly polarised light propagates through the plasma, its plane of polarisation is rotated by some some angle, β, given by:

$$\beta = RM\lambda^2 \tag{2}$$

where λ is the wavelength of the photon and RM is the rotation measure, given by:

$$RM = \frac{e^3}{2\pi^2 \epsilon_0 m^2 c^3} \int_0^d n_e(s) B_\parallel(s) ds \tag{3}$$

The angle of rotation therefore depends on the electron density, n_e in the plasma, the component of the magnetic field parallel to the direction of propagation of the photon, $B_\parallel$ and the photon's wavelength, λ.

Measurements of Faraday rotation within galaxy clusters have found the magnetic field strength to lie in the range of 0.2 - 3 μG [3]. In additon, Faraday rotation measurements yield magnetic field strengths in galaxies as 4 - 6 μG for spiral galaxies and 6 - 8 μG in elliptical and irregular galaxies [3].

Galactic Dynamos

On their own, seed magnetic fields such as PMFs are too weak (of order nanoguass) to give rise to the magnetic fields we see in the cosmos today. There must be a process for amplifying the seed magnetic fields.
Galactic dynamos are good candidates for seed magnetic field amplifiers. Dynamos are systems that convert kinetic energy into electromagnetic energy. Hot ionised gas rotates

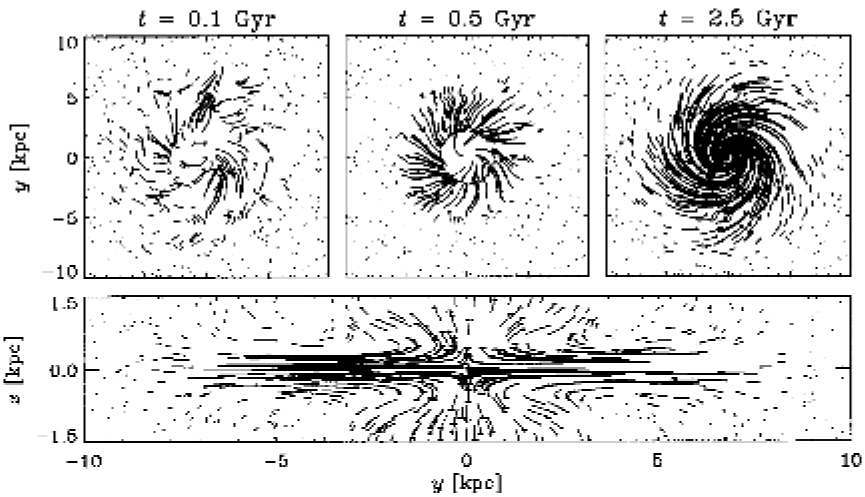

Figure 1: Spin up of magnetic fields in the presence of a galactic dynamo. In the first panel, at t = 0.1 Gyr, the seed magnetic field is picked up by a dynamo. Over the next two panels the dynamo spins up the magnetic field, increasing flux density. The bottom panel is a side-on view of the galactic dynamo at 8.1 Gyr. Figure from Beck et al., (1996) [4].

around the galactic centre of a galaxy. The ions drag the magnetic field lines along with them, tangling them up and increasing the magnetic flux density, and in addition the magnetic field strength. Hence galactic dynamos are able to amplify a weak seed magnetic field into a stronger magnetic field that we observe today.

1.2 CMB Polarisation

In the few years CMB polarisation has proven a powerful tool for studying large scale strucutre and the early Universe. If PMFs did in fact exist, then their traces ought to be found within the CMB polarisation. Section 2 contains a discussion on how PMFs affect CMB polarisation.

The CMB is the light from the Big Bang, however the CMB itself didn't form until 300,000 years after the Big Bang. At this point in time the Universe was cool enough to allow photons to decouple from baryons. This event is known as last-scattering. From there on the photons were able to free stream through the cosmos. Over the intervening 13 billion years the CMB photons have been cosmologically redshifted into the microwave frequency band. The CMB is a blackbody spectrum corresponding to a temperature of 2.73K.

The polarisation of the CMB first arose due to quadrupolar temperature anisotropies at last scattering [5]. Thomson scattering of photons in the electron-photon plasma linearly polarises out-going photons, however without anisotropies or only dipolar anisotropies, the net polarisation of the CMB is cancelled out. An electron in the plasma is surrounded by two hot regions and two cool regions oriented perpendicular to one another. Photons approaching from the hotter region impart their polarisation more strongly than those from cooler regions, producing net polarisations over patches of the sky. Figure 1 shows a diagram of Thomson scattering in a region with quadrupolar anisotropy.

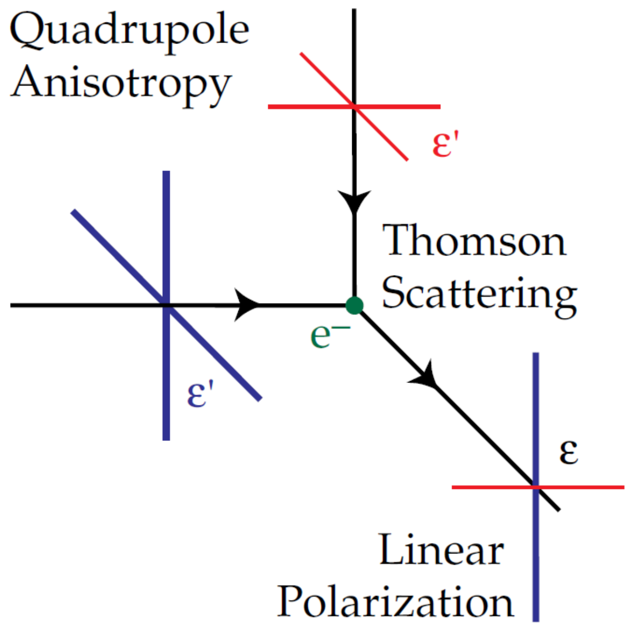

Figure 2: Thomson scattering of CMB photons in the presence of a quadrupole anisotropy. The red lines are the polarisations of a cold photon and the blue lines are the polarisations of a hot photon both incident on the same electron. The result is a net linear polarisation. Figure from Hu., (1996) [5]

Quadrupolar anisotropies are caused by scalar, vector or tensor perturbations. Scalar perturbations are density fluctuations. Vector perturbations result from vortices in the photon-electron fluid or from more exotic phenomena, such as cosmic strings and other topologcal defects. Finally a tensor perturbation would be the result of gravity waves produced during cosmic inflation.

In order to describe the effects of perturbations on CMB polarisation we introduce two polarisation modes. E-modes and B-modes. E-modes are formed from scalar perturbations. The E-modes resemble electric fields in electromagnetism in the sense that they are curl-free. It is also useful to note that E-modes have even parity. B-modes on the other hand are formed from vector and tensor perturbations and are currently undetected. Continuing the electromagnetism analogy a B-mode resembles a magnetic field, in the sense that it is purely a curl field. B-modes have odd parity.

The causes of B-mode CMB polarisation are new frontiers in physics. There is a strong case to study CMB polarisation, in the hopes that we may shed some light on the exotic nature of the early Universe.

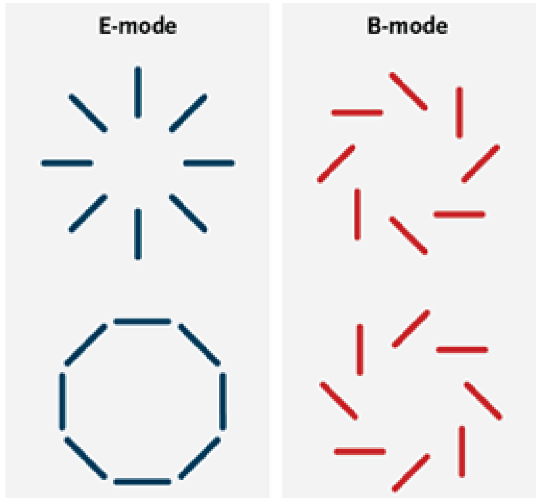

Figure 3: Representation of E-mode polarisations and B-mode polarisations. Note how E-modes are symmetric and resemble a divergent field. In contrast the B-modes appear anti-symmetric and resemble a curled field. Figure from Krauss, L. M., Dodelson, S., and Meyer, S., (2010) [6]

1.3 Future CMB experiments

This year stage-3 CMB experiments will commence operation and before the end of the next decade, stage-4 CMB experiments will have also collected their data. The next generation of CMB experiments aim to obtain tighter constraints on cosmological parameters such as the tensor-to-scalar ratio as well as map the CMB in higher detail than ever before. Though PMF detection is not the main science goal of these experiments, they will be able to tighten constraints on the primordial magnetic field strength and perhaps make a detection.

The key limitation in detecting PMFs will be the experimental senstivity, measured in noise (μK). To improve sensitivity one must decrease the noise, which is done by adding more detectors. The noise level and the number of detectors obey the relation:

$$noise \propto (\sqrt{n_{detectors}})^{-1}$$

Each stage of CMB experiments adds a factor of 10 more detectors, bringing the noise level down by a factor of $\sqrt{10}$.

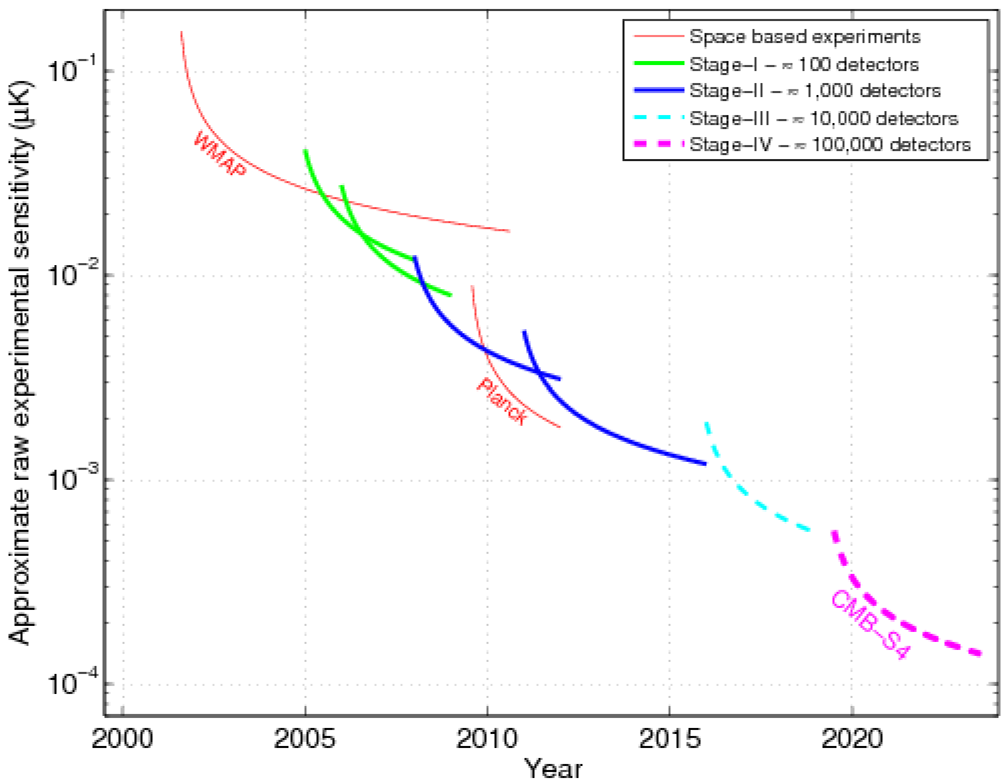

Figure 4: Plot of approximate raw experimental sensitivity of CMB experiments vs time in years. The Red lines indicate space-based experiments. Of note is PLANCK whose sensitivity falls in the middle-range of the stage-2 CMB experiments. The dotted cyan line represents the sensitivity of CMB-S3, which we expect to improve by up to an order of magnitude over Stage 2. CMB-S4 is represented by the dotted purple line, which is set to improve by a further order of magnitude over S3. Figure from Abazajian et. al., (2013) [7]

Table 1: Properties of Present and Future CMB experiments

Experiment	Stage	N_{bolo}	Scan Area (deg^2)	Polarisation Noise (μK)
SPT-pol	2	1536	100	20
PLANCK	2	detectors	Full Sky	noise
SPT-3G	3	15234	2500	4.8
Adv-ACTpol	3	2718	20 000	9.9
POLARBEAR2	3	7588		8.2
Simons Array	3	22764		4.8
Stage 4 Expected	4	500 000	20 000	1.4

This table shows a short (and by no means comprehensive) list of current and upcoming CMB experiments and their key design features useful for detecting PMFs. [8] [9] [10]

2 PMF Theory

2.1 Biermann Batteries

The large-scale magnetic fields we see need to have had some initial seed field, but of course this raises the question: Where did the seed field come from? The most popular model for seed magnetic field generation from zero initial conditions is the 'Biermann battery' proposed by Biermann in 1950. Biermann batteries form in highly ionised environments such as the plasma shortly afer the Big Bang. Within the plasma, ions are drawn to regions of lower density and lower temperature. Since the the constituents of the plasma - protons and electrons - have different masses they flow at different rates resulting in a net flow of charge. If this flow of current forms a loop, then by Faraday's law of induction, a magnetic field is produced by the battery.

The magnetic field produced by the Biermann battery is described by:

$$\frac{\partial \vec{B}}{\partial t} = \nabla \times (\vec{U} \times \vec{B} - \eta \nabla \times \vec{B}) - \frac{c k_b}{e} \frac{\nabla n_e}{n_e} \times \nabla T \tag{4}$$

The final term, $\nabla n_e \times \nabla T$ is the source term describing the Biermann battery effect. In order for this term to be non-zero and hence to have a Biermann battery, gradients of the electron density and the temperature must be non-parallel.

2.2 Other Methods of PMF Generation

Inflation

Cosmic inflation is an attactive model for PMF generation. During inflation the Universe isn't yet an ionised plasma. This means that the Universe is not a good conductor. In this state magnetic flux need not be conserved so it's possible for a seed field to emerge spontaneously.

The rapid expansion of the Universe in this epoch stretches out modes. Inflation stretches out quantum fluctuations into large scale density perturbations which seed the structure of the Universe. Similarly, inflation could stretch out small, weak magnetic fields to megaparsec scales as required.

A problem for this model is that it requires inflation to break conformal symmetry to produce this weak seed field initially. Turner and Widrow (1988) present one such model for conformal symmetry breaking leading to PMF generation in [11].

Phase Transitions

PMFs may have also been produced by early phase transitions, such as the QCD transition or the electroweak phase transition. During a phase transition bubbles of the new phase form within the previous phase, these bubbles grow and collide until the entire Universe reaches the lower phase. These phase transitions bring on non-equilibrium processes such as leptogenesis and baryogenesis, which may be responsible for producing some weak magnetic fields. Within a phase transition, a collision between bubbles will produce turbulence leading to dynamos which will serve to spin up the magnetic fields into the strengths required to match the field strengths observed today.

2.3 Effect of PMFs on the Cosmic Microwave Background

If PMFs have a field strength 1nG then their signatures will be detectable in the CMB B-mode polarisation power spectrum. Just as extragalactic magnetic fields Farday rotate radio and X-ray signals, PMFs would induce Faraday rotation within CMB polarisation. The net effect is that a fraction of E-mode polarisation would be transformed into B-mode polarisation. The PMF power spectrum is given by:

$$P(k) = A_{PMF} k^{n_B} \tag{5}$$

Where A_{PMF} is the PMF amplitude and n_B is the PMF spectral index. Since the scale of the PMF power spectrum will depend on the age of the Universe when they first formed, the spectral index is sensitive to the mechanism that first produced PMFs. If n_B... In order to measure the strength of PMFs we focus our attention to the amplitude, A_{PMF}. The PMF amplitude is related to B_{1Mpc}, the strength of PMFs coherent over 1 megaparsec by the following relation:

$$A_{PMF} \propto {B_{1Mpc}}^4 \tag{6}$$

Recent work from PLANCK (2015) has constrained the primordial magnetic field strength coherent over 1 Mpc to $B_{1Mpc} < 4.4$nG [12]. In 2016 POLARBEAR modestly improved this constraint to $B_{1Mpc} < 3.9$nG [13].

2.4 Other effects of PMFs

In addition to CMB polarisation, PMFs will affect the have effects on large scale structure and Big Bang Nucleosynthesis (BBN).

Large Scale Structure

PMFs can indirectly shape the the structure of the cosmos. At early times a PMF can exert a Lorentz force on baryonic matter. Since baryonic matter interacts gravitationally with dark matter, it follows that PMFs have an influence on matter distribution. This effect can be observed in the density perturbation amplitude over 8 Mpc, σ_8. One can also observe its effects by looking for changes in the matter power spectrum. Figure X shows the impact of PMFs on the matter power spectrum for Universes with either massless or massive neutrinos.

So far, there are no constraints on the PMF amplitude from large scale structure as the interactions happen in the non-linear regime, making measurements of its effects diffucult at the current time.

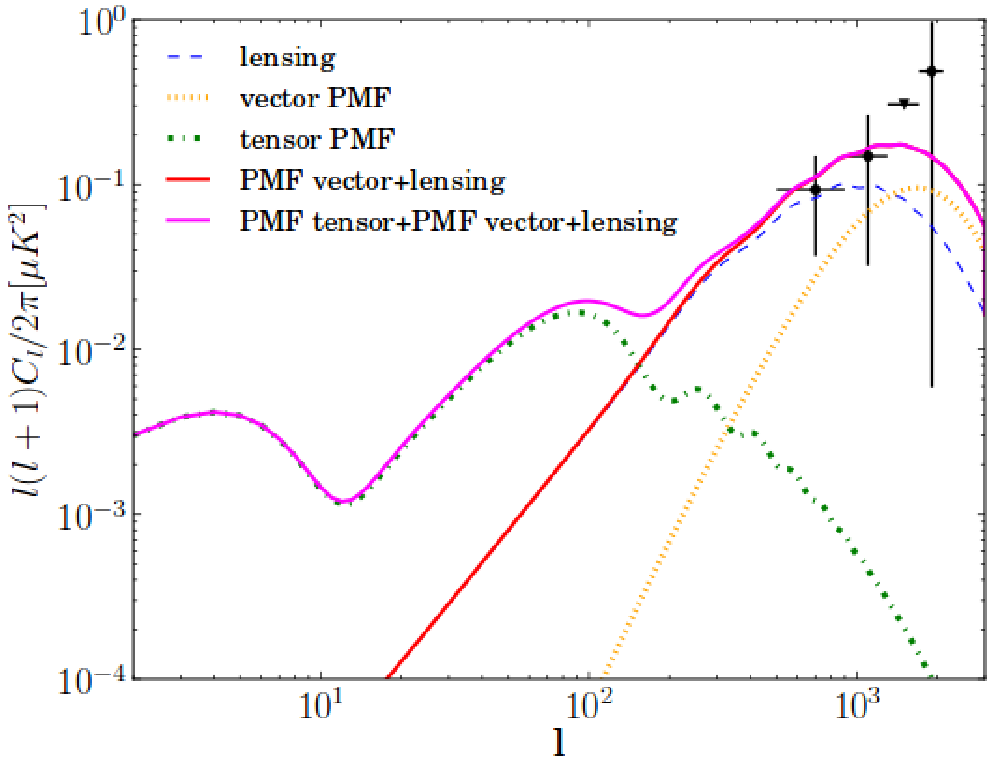

Figure 5: Plot of the CMB power spectrum. The dotted green and yellow lines show the power spectrum for vector and tensor PMFs. Vector PMFs have more power on smaller scales (larger ℓ) and tensor PMFs have more power on larger scales (smaller ℓ). The purple line shows the expected combined PMF plus lensing effects on the CMB. Compared to the blue dotted line for lensing alone, a PMF-influenced CMB power spectrum may be detectable on smaller scales than on larger scales.

Big Bang Nucleosynthesis

If PMFs existed prior to BBN then we expect to see its signature in nuclear abundances. Primordial magnetic fields contribute to the overall energy density of the Universe and therefore vary the rate of expansion. If the rates of expansion in the Universe differ then so does the rate at which the Universe cools. If PMFs were indeed formed prior to BBN then the freeze-out times of reactions during BBN would differ from standard model values and hence so would primordial abundances of Helium and Hydrogen.

The strongest constraints from BBN have $B_{1Mpc} < 1.5\ \mu G$ [14]. These constraints are far weaker than those currently given by CMB polarisation measurements.

2.5 Other Sources of Cosmic Birefringence

The rotation of E-mode polarisation to B-mode polarisation is not a phenomenon unique to PMFs. Another mechanism for this effect may be quintessence. Quintessence is an alternative

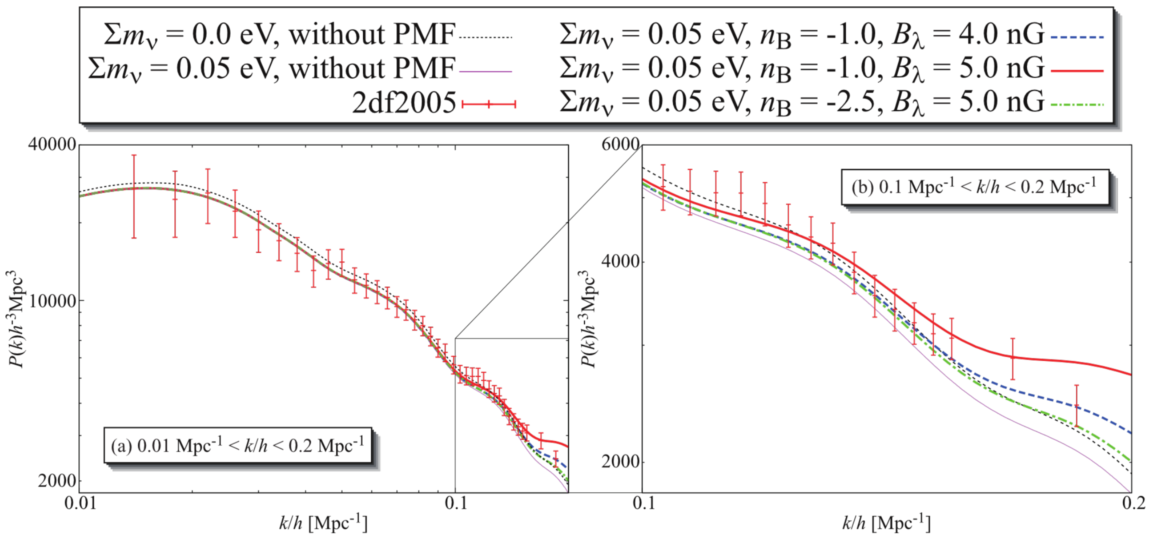

Figure 6: Plot of the matter power spectrum. Here B_λ is equal to B_{1Mpc} The left panel gives the power spectrum in the range $0.01Mpc^{-1} < k/h < 0.2Mpc^{-1}$. At small scales (small k/h) all models fall within the experimental error, however the Universe without massive neutrinos or PMFs has more power at these scales. The right panel gives the power spectrum in the range $0.1Mpc^{-1} < k/h < 0.2Mpc^{-1}$. At larger scales, the matter power spectrum is significantly affected by the presence and strength of PMFs.

explanation to the cosmological constant for the accelerating expansion of the Universe. It argues that there may exist a long-range pseudoscalar field that can very weakly couple to baryons. The interaction is described by the Chern-Simmons term:

$$\mathcal{L} \propto \frac{\phi}{2M} F_{\mu\nu}\tilde{F}^{\mu\nu} \tag{7}$$

Where ϕ is the pseudoscalar field and M is the mass of the field boson. If photons couple to this field, then their polarisation will be rotated, just as they would if there were a PMF. The rotation angle due to the pseudoscalar field is given by:

$$\alpha = \frac{1}{M}\int d\eta\dot{\phi} \tag{8}$$

Where $\dot{\phi}$ is integrated over the conformal time η

Currently we constrain the effects of cosmic birefringence with an equivalent effective PMF, however by comparing the two-point and four-point correlation functions it is possible to differentiate between effects due to PMFs and effects due to conjectured quintessence models. [13]

3 Method

In this section I outline the method I used to forecast upper limits for PMF detection using mock stage-3 and stage-4 covariance matrices and simulated CMB power spectra. In section 3.1 I will introduce the Fisher matrix, its properties and discuss how it is useful for experimental design. In section 3.2 I will discuss how I obtained CMB power spectra and how they are used to construct the Fisher matrix. Next, in section 3.3 I will describe the properties of the mock covariances and how I processed them into a useable format. Finally in section 3.4 will bring all the pieces together and explain how to obtain a Fisher matrix, apply conditioning to secure it against numerical instabilities and apply a change of variables to recieve forecasts for the upper limits on B_{1Mpc}.

3.1 Introduction to Fisher Matrices

The elements of the Fisher matrix are defined as:

$$\mathcal{F}_{ij} = -\left\langle \frac{\partial^2 ln\mathcal{L}}{\partial p^i \partial p^j} \right\rangle \tag{9}$$

where $\mathcal{L}$ is the likelihood and p^i, p^j are the i^{th} and j^{th} model parameters.

If the Fisher matrix is non-singular then it can be inverted into a covariance matrix for the model parameters. This result follows from the Cramèr-Rao theorem, which states that the variance of some unbiased estimator, p is greater than or equal to the inverse of its Fisher information. The Fisher information of a model parameter is given by:

$$F = -\langle \frac{\partial^2 ln\mathcal{L}}{\partial p^2} \rangle \tag{10}$$

Since the Fisher matrix can be inverted into a covariance matrix over the model parameters, it is a powerful tool in experimental design used for forecasting the upper limits on the precision of an experiment. The Fisher matrix has a number of useful properties:

Firstly, it is linear under addition: Adding n Fisher matrices returns a new Fisher matrix which can be inverted into a new covariance matrix with tighter constraints. This result is especially useful when you wish to know the total accuracy of many combined experiments.

$$(\mathcal{F}_1 + \mathcal{F}_2 + ... + \mathcal{F}_n)^{-1} = \mathcal{F}^{-1}_{1+2+...+n} \tag{11}$$

As a corollary, the Fisher matrix can be multiplied by a scalar, which is useful when you want to know the effect of repeating your experiment or adding more instances of the same design.

Furthermore, one can use this property to add priors to your design: suppose we know that one model parameter has been well-constrained in the past and our experiment isn't set to improve upon this result. We can combine the prior result with our current Fisher matrix to provide tighter constraints, like so:

$$\begin{bmatrix} F_{aa} & F_{ab} & F_{ac} \\ F_{ba} & F_{bb} & F_{bc} \\ F_{ca} & F_{cb} & F_{cc} \end{bmatrix} + \begin{bmatrix} 0 & 0 & 0 \\ 0 & 0 & 0 \\ 0 & 0 & P \end{bmatrix}$$

Here, we have a prior, P on variable c. All we need to do is add P to the corresponding diagonal term. However, if the prior is too big the Fisher matrix becomes singular. To combat this we employ the second useful property of Fisher matrices, marginalisation.

If we have a Fisher matrix with more variables than we're interested in, we can just throw away the rows and columns associated with the variables that we don't care about. The resultant matrix is a Fisher matrix that is valid for the remaining variables - there's no need to recalculate the Fisher matrix with fewer variables!

Returning to the case where P >> F_{cc}, we can marginalise over the variable c by removing its associated rows and columns from the Fisher matrix. In this case the information lost is negligible, since the variance from our experiment was much larger than P's experiment anyway. In return, we now find we can forecast for the remaining variables.

Usually, the Fisher matrix is found by calculating the log-likelihood for the model parameters. This is done by making likelihood chains in Markov-chain-Monte-Carlo simulations however this is not the only approach. If your model parameters are unbiased and Gaussian distributed then the following definition for the Fisher matrix holds:

$$F_{ij} = \frac{\partial f}{\partial p^i} C^{-1} \frac{\partial f}{\partial p^j} \tag{12}$$

where f is the function that relates the model parameters to each other, C is the covariance matrix for(???) and p^i are the model parameters. In this thesis I will take f to be the CMB polarisation power spectrum, C_ℓ. Next, p will be the ΛCDM parameters as well as some additional parameters (see 3.X) and finally C are mock covariance matrices associated with CMB-S3-like and CMB-S4-like experiments. Equation (12) then becomes:

$$F_{ij} = \frac{\partial C_\ell}{\partial p^i} C^{-1} \frac{\partial C_\ell}{\partial p^j} \tag{13}$$

3.2 CMB power spectra

To begin constructing the Fisher matrix in the form given by (12), I first used CAMB to build the CMB power spectrum. [describe CAMB] [also cite CAMB]

To call on CAMB one first needs to define parameters. A quick summary of the parameters and their central values is given in table 2. The parameters I varied were the six ΛCDM model parameters: $\Omega_b h^2$, the baryonic density. $\Omega_c h^2$, the cold dark matter density. H_0, Hubble's constant. τ, the optical depth of reionisation. τ is a measure of approximately when reionisation occurred. n_s, the scalar spectral index for the primordial power spectrum, given by $P(k) = A_s k^{n_s - 1}$. A_s is the amplitude of the primordial power spectrum. In addition we also have: The running of the scalar index, n_{run}. The effective number of neutrinos, N_{eff} and the tensor-to-scalar ratio, r, which is used in constraining the effects of primordial gravity waves.

In order to differentiate the power spectrum as required by (12) I employ a numerical form of the derivative:

$$\frac{\partial C_\ell}{\partial p} \approx \frac{\Delta C_\ell}{\Delta p} \tag{14}$$

Table 2: CAMB Parameters and Values

Parameter	Value	Uncertainty	Step Size
$\Omega_b h^2$	0.02227716	0.00023	$\pm 8 \times 10^{-5}$
$\Omega_c h^2$	0.1184293	0.022	$\pm 10^{-3}$
H_0	67.86682	0.96	$\pm 8 \times 10^{-2}$
τ	0.06664549	0.019	$\pm 10^{-3}$
n_s	0.9682903	0.0062	$\pm 10^{-3}$
A_s	2.140509e-09	0.118	$\pm 9 \times 10^{-12}$
n_{run}	0.0	-	$\pm 2 \times 10^{-3}$
N_{eff}	3.03066666667	0.23	$\pm 4 \times 10^{-3}$
r	0.01	-	$\pm 8 \times 10^{-4}$

This table shows the 6 ΛCDM model parameters, as well as the running of the scalar index, the effective number of neutrinos and the tensor-to-scalar ratio. The 'Value' column shows the central value I entered into CAMB when producing the polarisation power spectrum and the 'Step Size' column indicates the magnitude of the perturbation around the central value I used for calculating the numerical derivatives. Finally, the 'Uncertianty' column gives the PLANCK best fit (2015) [15] ΛCDM uncertainties, which were used as an upper bound for step sizes.

Where $\Delta C_\ell = C_\ell^{upper} - C_\ell^{lower}$ and $\Delta p = p^{upper} - p^{lower}$. To calculate ΔC_ℓ I call two instances of CAMB. In the first instance I add small perturbations to the central values (see table 2). The output power spectrum is called C_ℓ^{upper}. The second instance, C_ℓ^{lower} has small perturbations subtracted from the central values. Finally, Δp is equal to two times the perturbation values given in table 2.

To ensure that the derivatives are accurate the step sizes must be small, however if the step size is too small, the derivatives are subject to numerical artifacts. To choose well-conditioned step sizes I isolated each variable and generated a set of ΔC_ℓs while holding all other parameters fixed and varying the step size. To compare the step sizes I then plotted each family of ΔC_ℓ. When choosing a step size I looked for two things:

1. Convergence: As the step size approaches the best value, ΔC_ℓ will lose sensitivity to changes in step-size and the functions will converge to the same values for all ℓ.

2. Smoothness: If the step size is too small then ΔC_ℓ will oscillate significantly over a short change in ℓ. The resultant plot will look 'blocky' or have large spikes and won't resemble a well-conditioned derivative of the CMB power spectrum.

As a final sanity check on the value of the step sizes, I would like them to be less than the 2015 PLANCK best fit uncertainties (refer to table 2).
Figure 7 shows a plot of ΔC_ℓ for the BB polarisation power spectrum, varying Hubble's constant and holding all else fixed. The top panel shows the differences over $0 < \ell < 5000$. The lines all appear to be converging on the same function. The blue line, corresponding to a step size of 0.02 has significant artifacting, so by criterion one it can be ruled out. The

second panel is zoomed in on the peak and trough over ℓ 700. Taking a closer look at the lines reveals that as the step size increases toward 0.1 the lines begin to converge. There isn't an ostensible difference between step sizes of 0.08 or 0.1, so the deciding factor is which one produces a better approximation of $\frac{\partial C_\ell}{\partial p}$. Smaller step sizes suit this purpose so for Hubble's constant I chose 0.08.

An interesting second case is the difference plot for the tensor-to-scalar ratio. When $\ell < 220$ the difference plot is well behaved with good convergence and few artifacts for larger step sizes. When $\ell > 220$ numerical effects begin to dominate.

3.3 Covariance Matrix

For the inverse covariance matrix in (12) I used mock stage-3 and stage-4-like covariance matrices. These covariance matrices were calculated as per Tegmark (1997) [**?**] with five experimental parameters: Scan area, noise, ℓ_{knee}, beam error and calibration error. The values for these parameters match up with various stage-3 and stage-4 experimental designs.

- Scan area is the area of sky that these experiments will observe given in square degrees. For reference SPT-3G will observe a $2500deg^2$ patch of sky whereas PLANCK observed the whole sky.
- Noise is the background/instrumental(?) noise level of the experiment. This parameter is directly related to the number of bolometers in the experiment.
- ℓ_{knee} is the angular scale where $1/f$ noise starts dominating over the white noise. It is a measure of stability of the experiment and typically larger ℓ_{knee}s equal lower precision on CMB experiments.
- Beam error is the percentage error on the width of the beam. The width of the beam is given by its fwhm.
- Calibration error is the percentage error on the detectors.

In addition to the parameters the covariance matrix also has a prescribed binning. This isn't already implemented so it must be added manually. In order to bin the covariance matrix - and also the templates, I construct a bin matrix. The components of the bin matrix are defined like so:

$$B_{ij} = \begin{cases} (\Delta\ell)^{-1}, & \text{if } j\Delta\ell \leq i \leq (j+1)\Delta\ell \\ 0, & \text{otherwise} \end{cases} \tag{15}$$

Where $\Delta\ell$ is the length of the bin matrix and $j \leq N_{bin}$, the number of bins. This choice of binning takes the average of the derivative of the power spectrum over each bin.

The bin matrix is then applied to the inverse covariance matrix like so:

$$C^{-1}_{binned} = B^T C^{-1} B \tag{16}$$

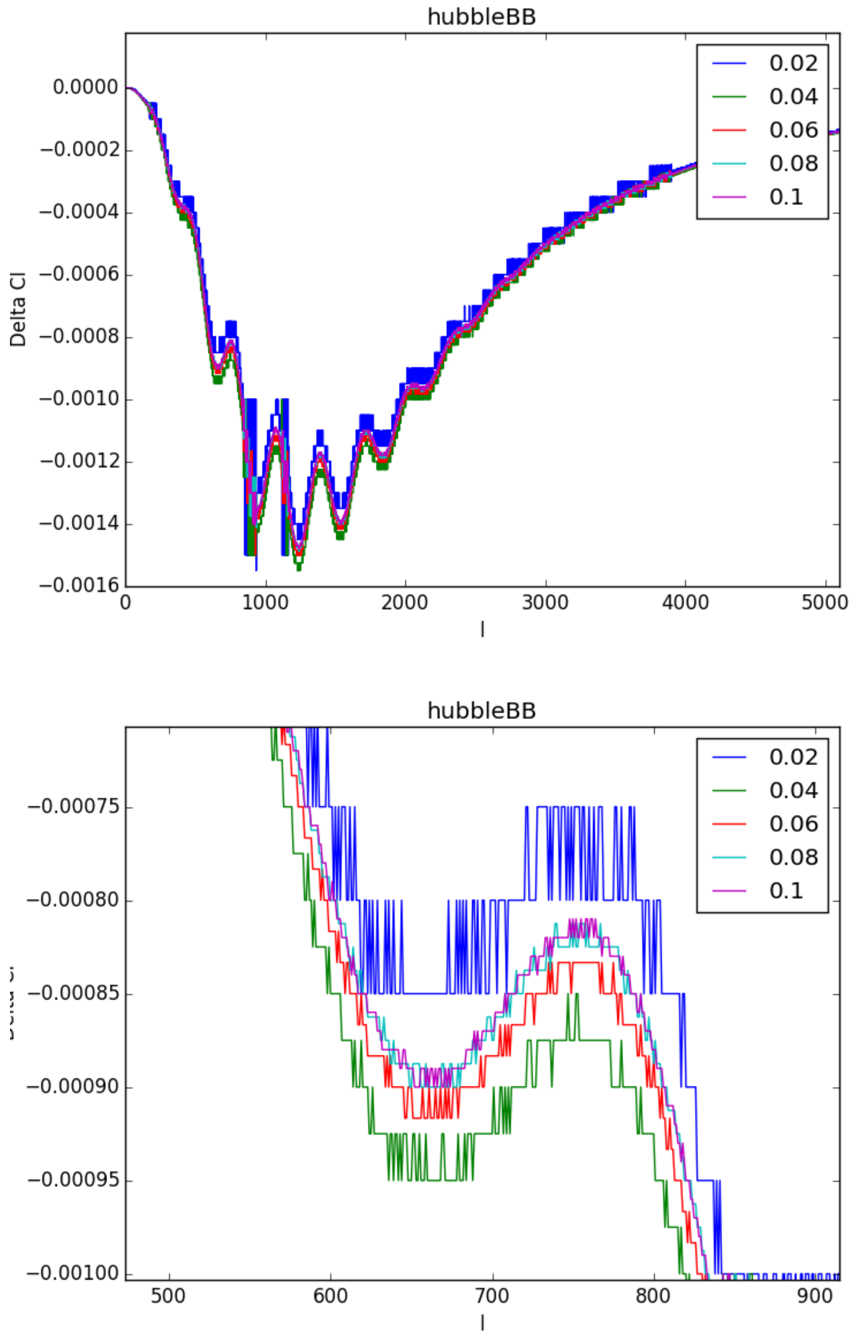

Figure 7: placeholder

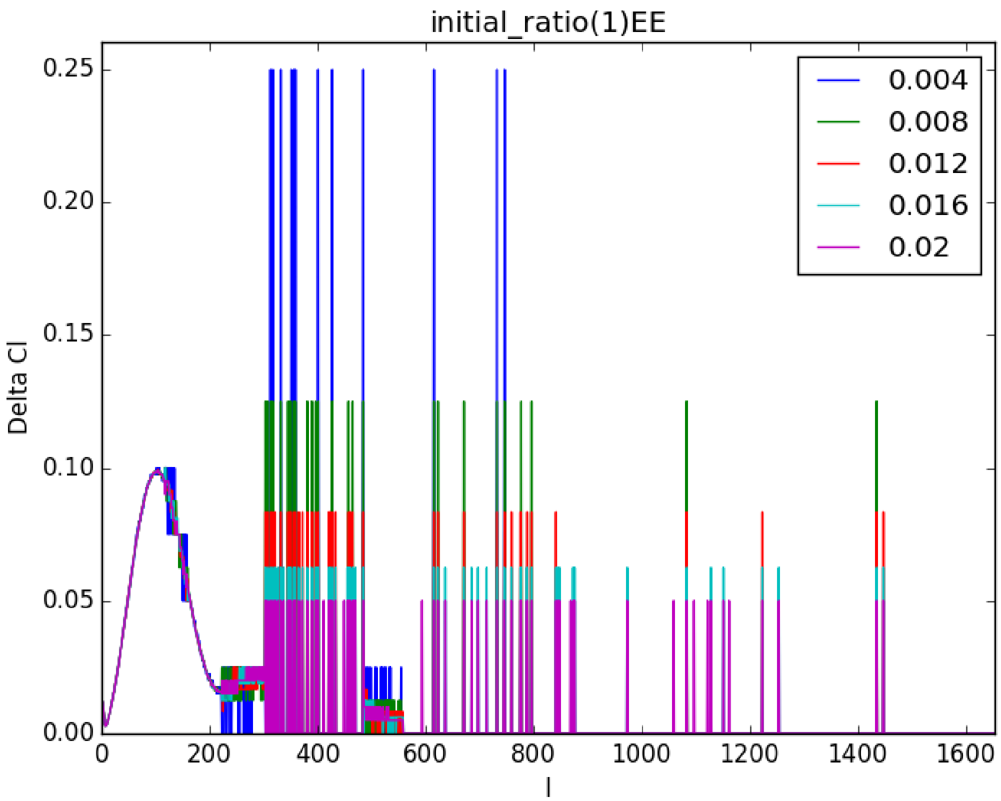

Figure 8: placeholder

Where B is the binning matrix, defined above and C^{-1} is the inverse covariance matrix. The templates are also binned like so:

$$(\frac{\partial C_\ell}{\partial p})_{binned} = B\frac{\partial C_\ell}{\partial p} \tag{17}$$

These new binned definitions are then substituted into (12) to construct the Fisher matrix. The output is an $N \times N$ matrix, where N is the number of parameters in the template matrix.

3.4 Constructing the Fisher Matrix

3.5 tests

4 Forecasts

4.1 ΛCDM forecasts

4.2 extended models

5 Discussion and Future Work

5.1 Discussion

5.2 Applications

5.3 Future Work

References

[1] T. Robishaw, E. Quataert, and C. Heiles, "Extragalactic Zeeman Detections in OH Megamasers," *Astrophys. J.*, vol. 680, p. 981, 2008.

[2] M. Giovannini, "The Magnetized universe," *Int. J. Mod. Phys.*, vol. D13, pp. 391–502, 2004.

[3] L. M. Widrow, "Origin of galactic and extragalactic magnetic fields," *Rev. Mod. Phys.*, vol. 74, pp. 775–823, 2002.

[4] R. Beck, A. Brandenburg, D. Moss, A. Shukurov, and D. Sokoloff

[5] W. Hu and M. J. White, "A CMB polarization primer," *New Astron.*, vol. 2, p. 323, 1997.

[6] L. Krauss, S. Dodelson, and S. Meyer, "Primordial gravitational waves and cosmology," *Science*, vol. 328, pp. 989–992, 5 2010.

[7] K. N. Abazajian *et al.*, "Neutrino Physics from the Cosmic Microwave Background and Large Scale Structure," *Astropart. Phys.*, vol. 63, pp. 66–80, 2015.

[8] S. W. Henderson *et al.*, "Advanced ACTPol Cryogenic Detector Arrays and Readout," *J. Low. Temp. Phys.*, vol. 184, no. 3-4, pp. 772–779, 2016.

[9] B. A. Benson *et al.*, "SPT-3G: A Next-Generation Cosmic Microwave Background Polarization Experiment on the South Pole Telescope," *Proc. SPIE Int. Soc. Opt. Eng.*, vol. 9153, p. 91531P, 2014.

[10] A. Suzuki *et al.*, "The POLARBEAR-2 and the Simons Array Experiment," *J. Low. Temp. Phys.*, vol. 184, no. 3-4, pp. 805–810, 2016.

[11] M. S. Turner and L. M. Widrow, "Inflation-produced, large-scale magnetic fields," *Phys. Rev. D*, vol. 37, pp. 2743–2754, May 1988.

[12] P. A. R. Ade *et al.*, "Planck 2015 results. XIX. Constraints on primordial magnetic fields," 2015.

[13] P. A. R. Ade *et al.*, "POLARBEAR Constraints on Cosmic Birefringence and Primordial Magnetic Fields," *Phys. Rev.*, vol. D92, p. 123509, 2015.

[14] M. Kawasaki and M. Kusakabe, "Updated constraint on a primordial magnetic field during big bang nucleosynthesis and a formulation of field effects," *Phys. Rev. D*, vol. 86, p. 063003, Sep 2012.

[15] P. A. R. Ade *et al.*, "Planck 2015 results. XIII. Cosmological parameters," 2015.